

Study of $e^+e^- \rightarrow \omega\chi_{cJ}$ at center-of-mass energies from 4.21 to 4.42 GeV

M. Ablikim¹, M. N. Achasov^{8,a}, X. C. Ai¹, O. Albayrak⁴, M. Albrecht³, D. J. Ambrose⁴², A. Amoroso^{46A,46C}, F. F. An¹, Q. An⁴³, J. Z. Bai¹, R. Baldini Ferroli^{19A}, Y. Ban³⁰, D. W. Bennett¹⁸, J. V. Bennett⁴, M. Bertani^{19A}, D. Bettoni^{20A}, J. M. Bian⁴¹, F. Bianchi^{46A,46C}, E. Boger^{22,g}, O. Bondarenko²⁴, I. Boyko²², R. A. Briere¹, H. Cai⁴⁸, X. Cai¹, O. Cakir^{38A}, A. Calcaterra^{19A}, G. F. Cao¹, S. A. Cetin^{38B}, J. F. Chang¹, G. Chelkov^{22,b}, G. Chen¹, H. S. Chen¹, H. Y. Chen², J. C. Chen¹, M. L. Chen¹, S. J. Chen²⁸, X. Chen¹, X. R. Chen²⁵, Y. B. Chen¹, H. P. Cheng¹⁶, X. K. Chu³⁰, Y. P. Chu¹, G. Cibinetto^{20A}, D. Cronin-Hennessy⁴¹, H. L. Dai¹, J. P. Dai¹, D. Dedovich²², Z. Y. Deng¹, A. Denig²¹, I. Denysenko²², M. Destefanis^{46A,46C}, F. De Mori^{46A,46C}, Y. Ding²⁶, C. Dong²⁹, J. Dong¹, L. Y. Dong¹, M. Y. Dong¹, S. X. Du⁵⁰, P. F. Duan¹, J. Z. Fan³⁷, J. Fang¹, S. S. Fang¹, X. Fang⁴³, Y. Fang¹, L. Fava^{46B,46C}, F. Feldbauer²¹, G. Felici^{19A}, C. Q. Feng⁴³, E. Fioravanti^{20A}, C. D. Fu¹, Q. Gao¹, Y. Gao³⁷, I. Garzia^{20A}, K. Goetzen⁹, W. X. Gong¹, W. Gradl²¹, M. Greco^{46A,46C}, M. H. Gu¹, Y. T. Gu¹¹, Y. H. Guan¹, A. Q. Guo¹, L. B. Guo²⁷, T. Guo²⁷, Y. Guo¹, Y. P. Guo²¹, Z. Haddadi²⁴, A. Hafner²¹, S. Han⁴⁸, Y. L. Han¹, F. A. Harris⁴⁰, K. L. He¹, Z. Y. He²⁹, T. Held³, Y. K. Heng¹, Z. L. Hou¹, C. Hu²⁷, H. M. Hu¹, J. F. Hu^{46A}, T. Hu¹, Y. Hu¹, G. M. Huang⁵, G. S. Huang⁴³, H. P. Huang⁴⁸, J. S. Huang¹⁴, X. T. Huang³², Y. Huang²⁸, T. Hussain⁴⁵, Q. Ji¹, Q. P. Ji²⁹, X. B. Ji¹, X. L. Ji¹, L. L. Jiang¹, L. W. Jiang⁴⁸, X. S. Jiang¹, J. B. Jiao³², Z. Jiao¹⁶, D. P. Jin¹, S. Jin¹, T. Johansson⁴⁷, A. Julin⁴¹, N. Kalantar-Nayestanaki²⁴, X. L. Kang¹, X. S. Kang²⁹, M. Kavatsyuk²⁴, B. C. Ke⁴, R. Kliemt¹³, B. Kloss²¹, O. B. Kolcu^{38B,c}, B. Kopf³, M. Kornicer⁴⁰, W. Kuehn²³, A. Kupsc⁴⁷, W. Lai¹, J. S. Lange²³, M. Lara¹⁸, P. Larin¹³, Cheng Li⁴³, C. H. Li¹, D. M. Li⁵⁰, F. Li¹, G. Li¹, H. B. Li¹, J. C. Li¹, Jin Li³¹, K. Li¹², K. Li³², P. R. Li³⁹, T. Li³², W. D. Li¹, W. G. Li¹, X. L. Li³², X. M. Li¹¹, X. N. Li¹, X. Q. Li²⁹, Z. B. Li³⁶, H. Liang⁴³, Y. F. Liang³⁴, Y. T. Liang²³, G. R. Liao¹⁰, D. X. Lin¹³, B. J. Liu¹, C. L. Liu⁴, C. X. Liu¹, F. H. Liu³³, Fang Liu¹, Feng Liu⁵, H. B. Liu¹¹, H. H. Liu¹, H. H. Liu¹⁵, H. M. Liu¹, J. Liu¹, J. P. Liu⁴⁸, J. Y. Liu¹, K. Liu³⁷, K. Y. Liu²⁶, L. D. Liu³⁰, Q. Liu³⁹, S. B. Liu⁴³, X. Liu²⁵, X. X. Liu³⁹, Y. B. Liu²⁹, Z. A. Liu¹, Zhiqiang Liu¹, Zhiqing Liu²¹, H. Loehner²⁴, X. C. Lou^{1,d}, H. J. Lu¹⁶, G. G. Lu¹, R. Q. Lu¹⁷, Y. Lu¹, Y. P. Lu¹, C. L. Luo²⁷, M. X. Luo⁴⁹, T. Luo⁴⁰, X. L. Luo¹, M. Lv¹, X. R. Lyu³⁹, F. C. Ma²⁶, H. L. Ma¹, L. L. Ma³², Q. M. Ma¹, S. Ma¹, T. Ma¹, X. N. Ma²⁹, X. Y. Ma¹, F. E. Maas¹³, M. Maggiora^{46A,46C}, Q. A. Malik⁴⁵, Y. J. Mao³⁰, Z. P. Mao¹, S. Marcello^{46A,46C}, J. G. Messchendorp²⁴, J. Min¹, T. J. Min¹, R. E. Mitchell¹⁸, X. H. Mo¹, Y. J. Mo⁵, H. Moeini²⁴, C. Morales Morales¹³, K. Moriya¹⁸, N. Yu. Muchnoi^{8,a}, H. Muramatsu⁴¹, Y. Nefedov²², F. Nerling¹³, I. B. Nikolaev^{8,a}, Z. Ning¹, S. Nisar⁷, S. L. Niu¹, X. Y. Niu¹, S. L. Olsen³¹, Q. Ouyang¹, S. Pacetti^{19B}, P. Patteri^{19A}, M. Pelizaeus³, H. P. Peng⁴³, K. Peters⁹, J. L. Ping²⁷, R. G. Ping¹, R. Poling⁴¹, Y. N. Pu¹⁷, M. Qi²⁸, S. Qian¹, C. F. Qiao³⁹, L. Q. Qin³², N. Qin⁴⁸, X. S. Qin¹, Y. Qin³⁰, Z. H. Qin¹, J. F. Qiu¹, K. H. Rashid⁴⁵, C. F. Redmer²¹, H. L. Ren¹⁷, M. Ripka²¹, G. Rong¹, X. D. Ruan¹¹, V. Santoro^{20A}, A. Sarantsev^{22,e}, M. Savrié^{20B}, K. Schoenning⁴⁷, S. Schumann²¹, W. Shan³⁰, M. Shao⁴³, C. P. Shen², P. X. Shen²⁹, X. Y. Shen¹, H. Y. Sheng¹, M. R. Shepherd¹⁸, W. M. Song¹, X. Y. Song¹, S. Sosio^{46A,46C}, S. Spataro^{46A,46C}, B. Spruck²³, G. X. Sun¹, J. F. Sun¹⁴, S. S. Sun¹, Y. J. Sun⁴³, Y. Z. Sun¹, Z. J. Sun¹, Z. T. Sun¹⁸, C. J. Tang³⁴, X. Tang¹, I. Tapan^{38C}, E. H. Thorndike⁴², M. Tiemens²⁴, D. Toth⁴¹, M. Ullrich²³, I. Uman^{38B}, G. S. Varner⁴⁰, B. Wang²⁹, B. L. Wang³⁹, D. Wang³⁰, D. Y. Wang³⁰, K. Wang¹, L. L. Wang¹, L. S. Wang¹, M. Wang³², P. Wang¹, P. L. Wang¹, Q. J. Wang¹, S. G. Wang³⁰, W. Wang¹, X. F. Wang³⁷, Y. D. Wang^{19A}, Y. F. Wang¹, Y. Q. Wang²¹, Z. Wang¹, Z. G. Wang¹, Z. H. Wang⁴³, Z. Y. Wang¹, D. H. Wei¹⁰, J. B. Wei³⁰, P. Weidenkaff²¹, S. P. Wen¹, U. Wiedner³, M. Wolke⁴⁷, L. H. Wu¹, Z. Wu¹, L. G. Xia³⁷, Y. Xia¹⁷, D. Xiao¹, Z. J. Xiao²⁷, Y. G. Xie¹, Q. L. Xiu¹, G. F. Xu¹, L. Xu¹, Q. J. Xu¹², Q. N. Xu³⁹, X. P. Xu³⁵, L. Yan⁴³, W. B. Yan⁴³, W. C. Yan⁴³, Y. H. Yan¹⁷, H. X. Yang¹, L. Yang⁴⁸, Y. Yang⁵, Y. X. Yang¹⁰, H. Ye¹, M. Ye¹, M. H. Ye⁶, J. H. Yin¹, B. X. Yu¹, C. X. Yu²⁹, H. W. Yu³⁰, J. S. Yu²⁵, C. Z. Yuan¹, W. L. Yuan²⁸, Y. Yuan¹, A. Yuncu^{38B,f}, A. A. Zafar⁴⁵, A. Zallo^{19A}, Y. Zeng¹⁷, B. X. Zhang¹, B. Y. Zhang¹, C. Zhang²⁸, C. C. Zhang¹, D. H. Zhang¹, H. H. Zhang³⁶, H. Y. Zhang¹, J. J. Zhang¹, J. L. Zhang¹, J. Q. Zhang¹, J. W. Zhang¹, J. Y. Zhang¹, J. Z. Zhang¹, K. Zhang¹, L. Zhang¹, S. H. Zhang¹, X. J. Zhang¹, X. Y. Zhang³², Y. Zhang¹, Y. H. Zhang¹, Z. H. Zhang⁵, Z. P. Zhang⁴³, Z. Y. Zhang⁴⁸, G. Zhao¹, J. W. Zhao¹, J. Y. Zhao¹, J. Z. Zhao¹, Lei Zhao⁴³, Ling Zhao¹, M. G. Zhao²⁹, Q. Zhao¹, Q. W. Zhao¹, S. J. Zhao⁵⁰, T. C. Zhao¹, Y. B. Zhao¹, Z. G. Zhao⁴³, A. Zhemchugov^{22,g}, B. Zheng⁴⁴, J. P. Zheng¹, W. J. Zheng³², Y. H. Zheng³⁹, B. Zhong²⁷, L. Zhou¹, Li Zhou²⁹, X. Zhou⁴⁸, X. K. Zhou⁴³, X. R. Zhou⁴³, X. Y. Zhou¹, K. Zhu¹, K. J. Zhu¹, S. Zhu¹, X. L. Zhu³⁷, Y. C. Zhu⁴³, Y. S. Zhu¹, Z. A. Zhu¹, J. Zhuang¹, B. S. Zou¹, J. H. Zou¹

(BESIII Collaboration)

¹ Institute of High Energy Physics, Beijing 100049, People's Republic of China

² Beihang University, Beijing 100191, People's Republic of China

³ Bochum Ruhr-University, D-44780 Bochum, Germany

⁴ Carnegie Mellon University, Pittsburgh, Pennsylvania 15213, USA

⁵ Central China Normal University, Wuhan 430079, People's Republic of China

⁶ China Center of Advanced Science and Technology, Beijing 100190, People's Republic of China

⁷ COMSATS Institute of Information Technology, Lahore, Defence Road, Off Raiwind Road, 54000 Lahore, Pakistan

⁸ G.I. Budker Institute of Nuclear Physics SB RAS (BINP), Novosibirsk 630090, Russia

⁹ GSI Helmholtzcentre for Heavy Ion Research GmbH, D-64291 Darmstadt, Germany

¹⁰ Guangxi Normal University, Guilin 541004, People's Republic of China

¹¹ GuangXi University, Nanning 530004, People's Republic of China

¹² Hangzhou Normal University, Hangzhou 310036, People's Republic of China

¹³ Helmholtz Institute Mainz, Johann-Joachim-Becher-Weg 45, D-55099 Mainz, Germany

¹⁴ Henan Normal University, Xinxiang 453007, People's Republic of China

- ¹⁵ Henan University of Science and Technology, Luoyang 471003, People's Republic of China
- ¹⁶ Huangshan College, Huangshan 245000, People's Republic of China
- ¹⁷ Hunan University, Changsha 410082, People's Republic of China
- ¹⁸ Indiana University, Bloomington, Indiana 47405, USA
- ¹⁹ (A)INFN Laboratori Nazionali di Frascati, I-00044, Frascati, Italy; (B)INFN and University of Perugia, I-06100, Perugia, Italy
- ²⁰ (A)INFN Sezione di Ferrara, I-44122, Ferrara, Italy; (B)University of Ferrara, I-44122, Ferrara, Italy
- ²¹ Johannes Gutenberg University of Mainz, Johann-Joachim-Becher-Weg 45, D-55099 Mainz, Germany
- ²² Joint Institute for Nuclear Research, 141980 Dubna, Moscow region, Russia
- ²³ Justus Liebig University Giessen, II. Physikalisches Institut, Heinrich-Buff-Ring 16, D-35392 Giessen, Germany
- ²⁴ KVI-CART, University of Groningen, NL-9747 AA Groningen, The Netherlands
- ²⁵ Lanzhou University, Lanzhou 730000, People's Republic of China
- ²⁶ Liaoning University, Shenyang 110036, People's Republic of China
- ²⁷ Nanjing Normal University, Nanjing 210023, People's Republic of China
- ²⁸ Nanjing University, Nanjing 210093, People's Republic of China
- ²⁹ Nankai University, Tianjin 300071, People's Republic of China
- ³⁰ Peking University, Beijing 100871, People's Republic of China
- ³¹ Seoul National University, Seoul, 151-747 Korea
- ³² Shandong University, Jinan 250100, People's Republic of China
- ³³ Shanxi University, Taiyuan 030006, People's Republic of China
- ³⁴ Sichuan University, Chengdu 610064, People's Republic of China
- ³⁵ Soochow University, Suzhou 215006, People's Republic of China
- ³⁶ Sun Yat-Sen University, Guangzhou 510275, People's Republic of China
- ³⁷ Tsinghua University, Beijing 100084, People's Republic of China
- ³⁸ (A)Ankara University, Dogol Caddesi, 06100 Tandogan, Ankara, Turkey; (B)Dogus University, 34722 Istanbul, Turkey; (C)Uludag University, 16059 Bursa, Turkey
- ³⁹ University of Chinese Academy of Sciences, Beijing 100049, People's Republic of China
- ⁴⁰ University of Hawaii, Honolulu, Hawaii 96822, USA
- ⁴¹ University of Minnesota, Minneapolis, Minnesota 55455, USA
- ⁴² University of Rochester, Rochester, New York 14627, USA
- ⁴³ University of Science and Technology of China, Hefei 230026, People's Republic of China
- ⁴⁴ University of South China, Hengyang 421001, People's Republic of China
- ⁴⁵ University of the Punjab, Lahore-54590, Pakistan
- ⁴⁶ (A)University of Turin, I-10125, Turin, Italy; (B)University of Eastern Piedmont, I-15121, Alessandria, Italy; (C)INFN, I-10125, Turin, Italy
- ⁴⁷ Uppsala University, Box 516, SE-75120 Uppsala, Sweden
- ⁴⁸ Wuhan University, Wuhan 430072, People's Republic of China
- ⁴⁹ Zhejiang University, Hangzhou 310027, People's Republic of China
- ⁵⁰ Zhengzhou University, Zhengzhou 450001, People's Republic of China
- ^a Also at the Novosibirsk State University, Novosibirsk, 630090, Russia
- ^b Also at the Moscow Institute of Physics and Technology, Moscow 141700, Russia and at the Functional Electronics Laboratory, Tomsk State University, Tomsk, 634050, Russia
- ^c Currently at Istanbul Arel University, Kucukcekmece, Istanbul, Turkey
- ^d Also at University of Texas at Dallas, Richardson, Texas 75083, USA
- ^e Also at the PNPI, Gatchina 188300, Russia
- ^f Also at Bogazici University, 34342 Istanbul, Turkey
- ^g Also at the Moscow Institute of Physics and Technology, Moscow 141700, Russia

Based on data samples collected with the BESIII detector at the BEPCII collider at 9 center-of-mass energies from 4.21 to 4.42 GeV, we search for the production of $e^+e^- \rightarrow \omega\chi_{cJ}$ ($J = 0, 1, 2$). The process $e^+e^- \rightarrow \omega\chi_{c0}$ is observed for the first time, and the Born cross sections at $\sqrt{s} = 4.23$ and 4.26 GeV are measured to be $(55.4 \pm 6.0 \pm 5.9)$ and $(23.7 \pm 5.3 \pm 3.5)$ pb, respectively, where the first uncertainties are statistical and the second are systematic. The $\omega\chi_{c0}$ signals at the other 7 energies and $e^+e^- \rightarrow \omega\chi_{c1}$ and $\omega\chi_{c2}$ signals are not significant, and the upper limits on the cross sections are determined. By examining the $\omega\chi_{c0}$ cross section as a function of center-of-mass energy, we find that it is inconsistent with the line shape of the $Y(4260)$ observed in $e^+e^- \rightarrow \pi^+\pi^-J/\psi$.

PACS numbers: 14.40.Rt, 13.66.Bc, 14.40.Pq, 13.25.Jx

The charmonium-like state $Y(4260)$ was first observed in its decay to $\pi^+\pi^-J/\psi$ [1], and has small

coupling to open charm decay modes [2]. Very recently, charged charmoniumlike states $Z_c(3900)$ [3–5], $Z_c(3885)$ [6], $Z_c(4020)$ [7, 8], and $Z_c(4025)$ [9] were observed in e^+e^- data collected around $\sqrt{s} = 4.26$ GeV. These features suggest the existence of a complicated substructure of the $Y(4260)$. Searches for new decay modes and measuring the line shape may provide information that is useful for understanding the nature of the $Y(4260)$.

Many theoretical models have been proposed to interpret the $Y(4260)$, *e.g.*, as a quark-gluon charmonium hybrid, a tetraquark state, a hadro-charmonium, or a hadronic molecule [10]. The authors of Ref. [11] predict a sizeable coupling between the $Y(4260)$ and the $\omega\chi_{c0}$ channel by considering the threshold effect of $\omega\chi_{c0}$ that plays a role in reducing the decay rates into open-charm channels. By adopting the spin rearrangement scheme in the heavy quark limit and the experimental information, Ref. [12] predicts the ratio of the decays $Y(4260) \rightarrow \omega\chi_{cJ}$ ($J = 0, 1, 2$) to be 4 : 3 : 5.

In this Letter, we report on the study of $e^+e^- \rightarrow \omega\chi_{cJ}$ ($J = 0, 1, 2$) based on the e^+e^- annihilation data samples collected with the BESIII detector operating at the BEPCII storage ring at 9 center-of-mass energy points in the range $\sqrt{s} = 4.21 - 4.42$ GeV. The BESIII detector is described in detail in Ref. [13]. In the analysis, the ω meson is reconstructed via its $\pi^+\pi^-\pi^0$ decay mode, the χ_{c0} state is reconstructed via $\pi^+\pi^-$ and K^+K^- decays, and the $\chi_{c1,2}$ states are reconstructed via $\chi_{c1,2} \rightarrow \gamma J/\psi$, $J/\psi \rightarrow \ell^+\ell^-$ ($\ell = e, \mu$).

GEANT4-based [14] Monte Carlo (MC) simulated samples, which are generated with EVTGEN [15] in conjunction with KKMC program [16], are used to optimize the selection criteria, determine the detector efficiency, and study the potential background. Each charged track is required to have a point of closest approach to the beamline that is within 1 cm in the radial direction and within 10 cm from the interaction point along the beam direction, and to have a polar angle that is well within the fiducial volume of main drift chamber (MDC), $|\cos\theta| < 0.93$ in laboratory frame. Photons are reconstructed from isolated showers in electromagnetic calorimeter (EMC) that are at least 10 degrees away from the nearest charged track. The photon energy is required to be at least 25 MeV in the barrel ($|\cos\theta| < 0.80$) and 50 MeV in the end-caps ($0.86 < |\cos\theta| < 0.92$). In order to suppress electronic noise and energy depositions that are unrelated to the event, the EMC time t of the photon candidates must be in coincidence with collision events within the range $0 \leq t \leq 700$ ns. A π^0 is reconstructed from its decay to two photons by requiring the invariant mass of two photons $M_{\gamma\gamma}$ to be in the mass interval $[0.110, 0.145]$ GeV/ c^2 , and a π^0 candidate list is formed by looping over all photon candidates.

A candidate event must have four tracks with zero net charge and at least one π^0 candidate; for the $e^+e^- \rightarrow \omega\chi_{c1,2}$ channels, an additional photon is required. The tracks with a momentum larger than 1 GeV/ c are iden-

tified as originating from χ_{cJ} , lower momentum pions are interpreted as originating from ω decays. A $5C$ kinematic fit is performed to constrain the total four-momentum of all particles in the final states to that of the initial e^+e^- system, and $M_{\gamma\gamma}$ is constrained to m_{π^0} . If more than one candidate occurs in an event, the one with the smallest χ_{5C}^2 of the kinematic fit is selected. For the channel $e^+e^- \rightarrow \omega\chi_{c0}$, the two tracks from the χ_{c0} are assumed to be $\pi^+\pi^-$ or K^+K^- pairs. If $\chi_{5C}^2(\pi^+\pi^-) < \chi_{5C}^2(K^+K^-)$, the event is identified as originating from the $\pi^+\pi^-$ mode, otherwise it is considered to be from the K^+K^- mode. χ_{5C}^2 is required to be less than 100. For the J/ψ reconstruction in the $e^+e^- \rightarrow \omega\chi_{c1,2}$ channels, we separate e from μ using the energy deposition in the EMC: for muon candidates it is required to be less than 0.4 GeV, while for electrons it is required to be larger than 1 GeV. The χ_{5C}^2 of the kinematic fit for the $\omega\chi_{c1,2}$ candidate event is required to be less than 60.

The background for the $e^+e^- \rightarrow \omega\chi_{c0}$ channel is studied by using MC samples obtained at $\sqrt{s} = 4.23, 4.26$, and 4.36 GeV which include the $Y(4260)$ resonance, initial state radiation (ISR) of the vector charmonium, and QED events. The main sources of background after event selection are found to be $e^+e^- \rightarrow \omega\pi^+\pi^-$ (ωK^+K^-), where the $\pi^+\pi^-$ (K^+K^-) are not from χ_{c0} decays. The scatter plots of the invariant mass of $\pi^+\pi^-\pi^0$ versus that of $\pi^+\pi^-$ or K^+K^- for data at $\sqrt{s} = 4.23$ and 4.26 GeV are shown in Fig. 1. Clear accumulations of events are seen around the intersections of the ω and χ_{c0} regions, which indicate $\omega\chi_{c0}$ signals. Signal candidates are required to be in the ω signal region, defined as $0.75 \leq M(\pi^+\pi^-\pi^0) \leq 0.81$ GeV/ c^2 where $M(\pi^+\pi^-\pi^0)$ is the invariant mass of $\pi^+\pi^-\pi^0$. The ω sideband is taken as $0.6 \leq M(\pi^+\pi^-\pi^0) \leq 0.72$ GeV/ c^2 to estimate the non-resonant background.

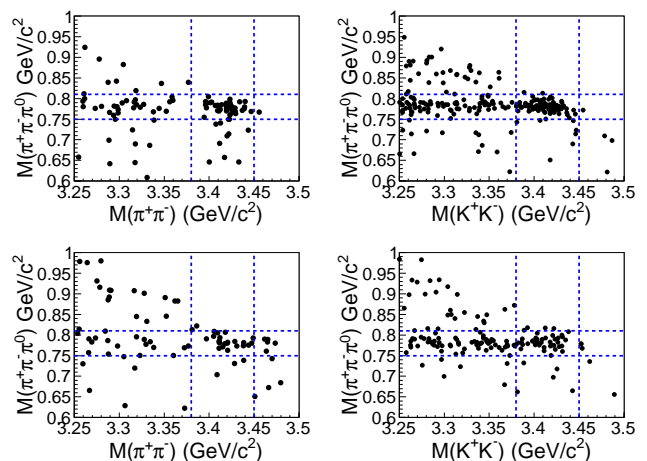


FIG. 1. Scatter plots of the $\pi^+\pi^-\pi^0$ invariant mass versus the $\pi^+\pi^-$ (left) and K^+K^- (right) invariant mass at $\sqrt{s} = 4.23$ GeV (top) and $\sqrt{s} = 4.26$ GeV (bottom). The dashed lines denote the ω and χ_{c0} signal regions.

Figure 2 shows $M(\pi^+\pi^-)$ and $M(K^+K^-)$ at $\sqrt{s} = 4.23$ and 4.26 GeV after all requirements are imposed. To extract the signal yield, an unbinned maximum likelihood fit is performed on the $\pi^+\pi^-$ and K^+K^- modes simultaneously. The signal is described with a shape determined from the simulated signal MC sample. The background is described with an ARGUS function, $m\sqrt{1 - (m/m_0)^2} \cdot e^{k(1 - (m/m_0)^2)}$ [17], where k is a free parameter in the fit, and m_0 is fixed at $\sqrt{s} - 0.75$ GeV (0.75 GeV is the lower limit of the $M(\pi^+\pi^-\pi^0)$ requirement). In the fit, the ratio of the number of $\pi^+\pi^-$ events to that of K^+K^- events is fixed to be $\frac{\epsilon_\pi \mathcal{B}(\chi_{c0} \rightarrow \pi^+\pi^-)}{\epsilon_K \mathcal{B}(\chi_{c0} \rightarrow K^+K^-)}$, where $\mathcal{B}(\chi_{c0} \rightarrow \pi^+\pi^-)$ and $\mathcal{B}(\chi_{c0} \rightarrow K^+K^-)$ are taken as world average values [18], and ϵ_π and ϵ_K are the efficiencies of $\pi^+\pi^-$ and K^+K^- modes determined from MC simulations, respectively. The possible interference between the signal and background is neglected. The fit results are shown in Fig. 2. For the $\sqrt{s} = 4.23$ GeV data, the total signal yield of the two modes is 125.3 ± 13.5 , and the signal statistical significance is 11.9σ . By projecting the events of the two modes into two histograms (at least 7 events per bin), the goodness-of-fit is found to be $\chi^2/\text{d.o.f.} = 37.6/22$, where the d.o.f. is the number of degrees of freedom. For the $\sqrt{s} = 4.26$ GeV data, the total signal yield is 45.5 ± 10.2 with a statistical significance of 5.5σ , and the goodness-of-the-fit is $\chi^2/\text{d.o.f.} = 27.1/15$. Since the statistics at the other energy points are very limited, the number of the observed events is obtained by counting the entries in the χ_{c0} signal region [3.38, 3.45] GeV/c^2 , and the number of background events in the signal region is obtained by fitting the $M(\pi^+\pi^-)$ [$M(K^+K^-)$] spectrum excluding the χ_{c0} signal region and scaling to the size of the signal region. The results at all the energy points are listed in Table I.

For the process $e^+e^- \rightarrow \omega\chi_{c1,2}$, the main remaining backgrounds stem from $e^+e^- \rightarrow \pi^+\pi^-\psi'$, $\psi' \rightarrow \pi^0\pi^0 J/\psi$ and $e^+e^- \rightarrow \pi^0\pi^0\psi'$, $\psi' \rightarrow \pi^+\pi^- J/\psi$. To suppress these backgrounds, we exclude events in which the invariant mass $M(\pi^+\pi^-\ell^+\ell^-)$ or the mass recoiling against $\pi^+\pi^-$ [$M^{\text{recoil}}(\pi^+\pi^-)$] lie in the region [3.68, 3.70] GeV/c^2 .

The J/ψ and ω signal regions are set to be [3.08, 3.12] GeV/c^2 and [0.75, 0.81] GeV/c^2 , respectively. After all the requirements are applied, no obvious signals are observed at $\sqrt{s} = 4.31, 4.36, 4.39,$ and 4.42 GeV. The number of observed events is obtained by counting events in the χ_{c1} or χ_{c2} signal regions, which are defined as [3.49, 3.53] or [3.54, 3.58] GeV/c^2 , respectively. The number of background events in the signal regions is estimated with data obtained from the sideband region [3.35, 3.47] GeV/c^2 in the $M(\gamma J/\psi)$ distribution by assuming a flat distribution in the full mass range. The number of observed events and estimated background events at each energy point are listed in Table II.

The Born cross section is calculated from

$$\sigma^{\text{B}} = \frac{N^{\text{obs}}}{\mathcal{L}(1 + \delta^r)(1 + \delta^v)(\epsilon_1 \mathcal{B}_1 + \epsilon_2 \mathcal{B}_2) \mathcal{B}_3}, \quad (1)$$

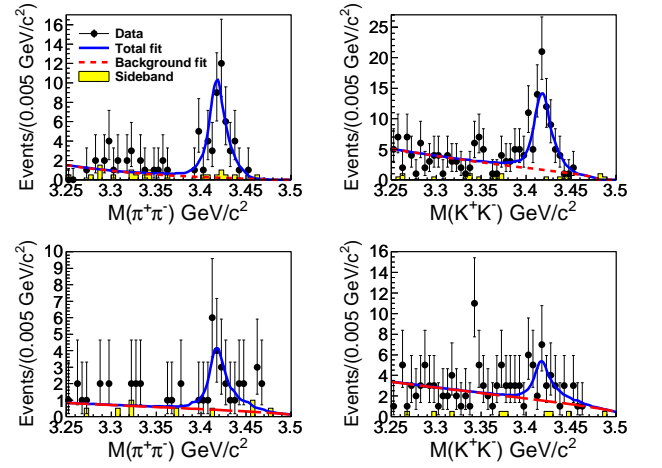


FIG. 2. Fit to the invariant mass distributions $M(\pi^+\pi^-)$ (left) and $M(K^+K^-)$ (right) after requiring $M(\pi^+\pi^-\pi^0)$ in the ω signal region. Points with error bars are data, the solid curves are the fit results, the dashed lines indicate the background and the shaded histograms show the normalized ω sideband events. The top two plots represent data at $\sqrt{s} = 4.23$ GeV, and the bottom two at $\sqrt{s} = 4.26$ GeV.

where N^{obs} is the number of observed signal events, \mathcal{L} is the integrated luminosity, $(1 + \delta^r)$ is the radiative correction factor which is obtained by using a QED calculation [19] and taking the cross section measured in this analysis with two iterations as input, $(1 + \delta^v)$ is the vacuum polarization factor which is taken from a QED calculation with an accuracy of 0.5% [20]. For the $e^+e^- \rightarrow \omega\chi_{c0}$ channel, $\mathcal{B}_1 = \mathcal{B}(\chi_{c0} \rightarrow \pi^+\pi^-)$, $\mathcal{B}_2 = \mathcal{B}(\chi_{c0} \rightarrow K^+K^-)$, $\mathcal{B}_3 = \mathcal{B}(\omega \rightarrow \pi^+\pi^-\pi^0) \times \mathcal{B}(\pi^0 \rightarrow \gamma\gamma)$, and ϵ_1 and ϵ_2 are the efficiencies for the $\pi^+\pi^-$ (ϵ_π) and K^+K^- (ϵ_K) modes, respectively. For the $e^+e^- \rightarrow \omega\chi_{c1,2}$ channels, $\mathcal{B}_1 = \mathcal{B}(J/\psi \rightarrow e^+e^-)$, $\mathcal{B}_2 = \mathcal{B}(J/\psi \rightarrow \mu^+\mu^-)$, $\mathcal{B}_3 = \mathcal{B}(\chi_{c1,2} \rightarrow \gamma J/\psi) \times \mathcal{B}(\omega \rightarrow \pi^+\pi^-\pi^0) \times \mathcal{B}(\pi^0 \rightarrow \gamma\gamma)$, ϵ_1 and ϵ_2 are the efficiencies of e^+e^- (ϵ_e) and $\mu^+\mu^-$ (ϵ_μ) modes, respectively.

For center of mass energies where the signal is not significant, we set upper limits at the 90% confidence level (C.L.) on the Born cross section. The upper limit is calculated by using a frequentist method with unbounded profile likelihood treatment of systematic uncertainties, which is implemented by a C++ class TROLKE in the ROOT framework [21]. The number of the observed events is assumed to follow a Poisson distribution, the number of background events and the efficiency are assumed to follow Gaussian distributions. In order to consider the systematic uncertainty in the calculation, we use the denominator in Eq. (1) as an effective efficiency as implemented in TROLKE.

The Born cross section or its upper limit at each energy point for $e^+e^- \rightarrow \omega\chi_{c0}$ and $e^+e^- \rightarrow \omega\chi_{c1,2}$ are listed in Tables I and II, respectively.

Figure 3 shows the measured Born cross sections for

TABLE I. The results on $e^+e^- \rightarrow \omega\chi_{c0}$. Shown in the table are the luminosity \mathcal{L} , product of radiative correction factor, branching fraction and efficiency $\mathcal{D} = (1 + \delta^r) \cdot (\epsilon_\pi \cdot \mathcal{B}(\chi_{c0} \rightarrow \pi^+\pi^-) + \epsilon_K \cdot \mathcal{B}(\chi_{c0} \rightarrow K^+K^-))$, number of observed events N^{obs} (the numbers of background are subtracted at $\sqrt{s} = 4.23$ and 4.26 GeV), number of estimated background N^{bkg} , vacuum polarization factor $(1 + \delta^v)$, Born cross section σ^{B} , and upper limit (at the 90% C.L.) on Born cross section $\sigma_{\text{UL}}^{\text{B}}$ at each energy point. The first uncertainty of the Born cross section is statistical, and the second systematic. The dashes mean not available.

\sqrt{s} (GeV)	\mathcal{L} (pb $^{-1}$)	\mathcal{D} ($\times 10^{-3}$)	N^{obs}	N^{bkg}	$1 + \delta^v$	σ^{B} (pb)	$\sigma_{\text{UL}}^{\text{B}}$ (pb)
4.21	54.6	1.99	7	5.0 ± 2.8	1.057	$20.2_{-37.7}^{+46.3} \pm 3.3$	< 90
4.22	54.1	2.12	7	4.3 ± 2.1	1.057	$25.1_{-30.4}^{+39.4} \pm 2.0$	< 81
4.23	1047.3	2.29	125.3 ± 13.5	—	1.056	$55.4 \pm 6.0 \pm 5.9$	—
4.245	55.6	2.44	6	4.0 ± 1.5	1.056	$16.3_{-22.3}^{+30.8} \pm 1.5$	< 60
4.26	826.7	2.50	45.5 ± 10.2	—	1.054	$23.7 \pm 5.3 \pm 3.5$	—
4.31	44.9	2.56	5	2.2 ± 1.6	1.053	$26.2_{-25.1}^{+34.9} \pm 2.2$	< 76
4.36	539.8	2.62	29	32.4 ± 4.7	1.051	$-2.6_{-5.4}^{+6.1} \pm 0.27$	< 6
4.39	55.2	2.57	2	0.6 ± 0.7	1.051	$10.4_{-11.2}^{+20.7} \pm 0.7$	< 37
4.42	44.7	2.46	0	1.4 ± 1.5	1.053	$-13.6_{-14.7}^{+18.5} \pm 1.3$	< 15

TABLE II. The results on $e^+e^- \rightarrow \omega\chi_{c1,2}$. Listed in the table are the product of radiative correction factor, branching fraction and efficiency $\mathcal{D} = (1 + \delta^r) \cdot (\epsilon_e \cdot \mathcal{B}(J/\psi \rightarrow e^+e^-) + \epsilon_\mu \cdot \mathcal{B}(J/\psi \rightarrow \mu^+\mu^-))$, number of the observed events N^{obs} , number of backgrounds N^{bkg} estimated from sideband regions, and the upper limit (at the 90% C.L.) on the Born cross section $\sigma_{\text{UL}}^{\text{B}}$.

Mode	\sqrt{s} (GeV)	\mathcal{D} ($\times 10^{-2}$)	N^{obs}	N^{bkg}	$\sigma_{\text{UL}}^{\text{B}}$ (pb)
$\omega\chi_{c1}$	4.31	1.43	1	0	< 18
	4.36	1.27	1	1	< 0.9
	4.39	1.27	1	0	< 17
	4.42	1.25	0	0	< 11
$\omega\chi_{c2}$	4.36	0.95	5	1	< 11
	4.39	1.06	3	0	< 64
	4.42	0.98	2	0	< 61

$e^+e^- \rightarrow \omega\chi_{c0}$ over the energy region studied in this work (we follow the convention to fit the dressed cross section $\sigma^{\text{B}} \cdot (1 + \delta^v)$ in extracting the resonant parameters in [18]). A maximum likelihood method is used to fit the shape of the cross section.

Assuming that the $\omega\chi_{c0}$ signals come from a single resonance, a phase-space modified Breit-Wigner (BW) function

$$\text{BW}(\sqrt{s}) = \frac{\Gamma_{ee}\mathcal{B}(\omega\chi_{c0})\Gamma_t}{(s - M^2)^2 + (M\Gamma_t)^2} \cdot \frac{\Phi(\sqrt{s})}{\Phi(M)} \quad (2)$$

is used to parameterize the resonance, where Γ_{ee} is the e^+e^- partial width, Γ_t the total width, and $\mathcal{B}(\omega\chi_{c0})$ the branching fraction of the resonance decay to $\omega\chi_{c0}$. $\Phi(\sqrt{s}) = \frac{P}{\sqrt{s}}$ is the phase space factor for an S -wave two-body system, where P is the ω momentum in the e^+e^- center-of-mass frame. We fit the data with a coherent sum of the BW function and a phase space term and find that the phase space term does not contribute significantly. The fit results for the resonance parameters are $\Gamma_{ee}\mathcal{B}(\omega\chi_{c0}) = (2.7 \pm 0.5)$ eV, $M = (4230 \pm 8)$ MeV/ c^2 , and $\Gamma_t = (38 \pm 12)$ MeV. Fitting the data using the only

phase space term results in a large change of the likelihood [$\Delta(-2 \ln L) = 101.6$]. Taking the change of 4 in the d.o.f.s into account, this corresponds to a statistical significance of $> 9\sigma$.

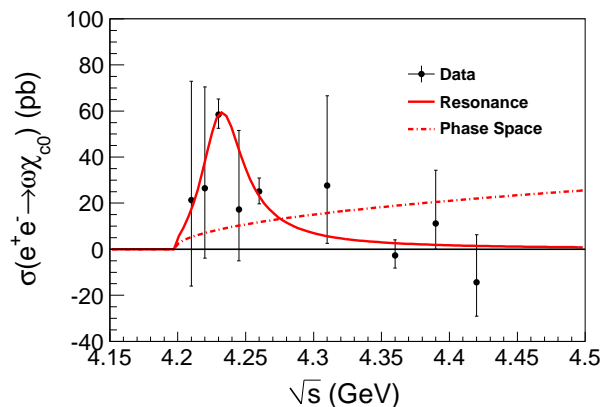


FIG. 3. Fit to $\sigma(e^+e^- \rightarrow \omega\chi_{c0})$ with a resonance (solid curve), or a phase space term (dot-dashed curve). Dots with error bars are the dressed cross sections. The uncertainties are statistical only.

The systematic uncertainties in the Born cross section measurement mainly originate from the luminosity measurement, the detection efficiency, the radiative correction, the fit procedure, and the intermediate decay branching fractions. The luminosity is measured by using Bhabha events with an uncertainty of 1.0%. The uncertainty in tracking efficiency is 1.0% per track. The uncertainty in photon reconstruction is 1.0% per photon, obtained by studying a large sample of $J/\psi \rightarrow \rho^0\pi^0$ decays [22]. The uncertainty in the kinematic fit is estimated by correcting the helix parameters of charged tracks according to the procedure described in Ref. [23]. The uncertainty in the radiative correction is estimated by varying the line shape of the cross section in the generator from the measured energy-dependent cross section

to the $Y(4260)$ Breit-Wigner shape. The polar angle θ of the ω in the e^+e^- center-of-mass frame is defined as the angle between ω and e^- beam. For the $\omega\chi_{c0}$ channel, the distribution of θ is obtained from data taken at 4.23 GeV and fitted with $1 + \alpha \cos^2 \theta$. The value of α is determined to be -0.28 ± 0.31 . The efficiencies are determined from MC simulations with $\alpha = -0.28$, and the uncertainty is estimated by varying α within one standard deviation. For the $\omega\chi_{c1,2}$ channels, the uncertainty is estimated by varying the ω angular distribution from flat to $1 \pm \cos^2 \theta$.

For the $e^+e^- \rightarrow \omega\chi_{c0}$ mode, the uncertainty due to cross feed between K^+K^- and $\pi^+\pi^-$ modes is estimated using the signal MC samples. The uncertainty in the fit procedure includes the fitting range, the mass resolution, the branching fractions of $\chi_{c0} \rightarrow \pi^+\pi^-$ and $\chi_{c0} \rightarrow K^+K^-$, and the background shape. The uncertainty from the fitting range is obtained by varying the limits of the fitting range by ± 0.05 GeV/ c^2 . The uncertainty from the mass resolution is determined to be negligible compared to the resolutions of the reconstructed ω in data and MC samples. The uncertainties associated with $\mathcal{B}(\chi_{c0} \rightarrow \pi^+\pi^-)$ and $\mathcal{B}(\chi_{c0} \rightarrow K^+K^-)$ are obtained by varying the branching fractions around their world average values by one standard deviation [18]. The systematic uncertainty due to the choice of the background shape is estimated by changing the background shape from the ARGUS function to a second order polynomial (where the parameters of the polynomial are allowed to float). Tables III summarizes the relative systematic errors for the $\omega\chi_{c0}$ channel. The overall systematic errors are obtained by summing all the sources of systematic uncertainties in quadrature by assuming they are independent.

The systematic uncertainties on the resonant parameters in the fit to the energy-dependent cross section of $e^+e^- \rightarrow \omega\chi_{c0}$ are mainly from the uncertainties of \sqrt{s} determination, energy spread, parametrization of the BW function, and the cross section measurement. The BEPC energy measurement system [24] measures beam energy with a precision of 1 MeV, resulting in the center-of-mass energy with a precision of 2 MeV. It is dominated by systematic uncertainties that are common to all the energy points. This introduces a ± 2 MeV/ c^2 uncertainty in the mass measurement. To estimate the uncertainty from the energy spread of \sqrt{s} (1.6 MeV), a BW function convoluted with a Gaussian function with a resolution of 1.6 MeV is used to fit the data, and the uncertainties are estimated by comparing the results with the nominal ones. Instead of using a constant total width, we assume a mass dependent width $\Gamma_t = \Gamma_t^0 \cdot \frac{\Phi(\sqrt{s})}{\Phi(M)}$, where Γ_t^0 is the width of the resonance, to estimate the systematic uncertainty due to signal parametrization. The systematic uncertainty of the Born cross section (except that from

$1 + \delta^v$) contributes uncertainty in $\Gamma_{ee}\mathcal{B}(\omega\chi_{c0})$. By adding all these sources of systematic uncertainties in quadrature, we obtain uncertainties of ± 6 MeV/ c^2 , ± 2 MeV, and ± 0.4 eV for the mass, width, and the partial width, respectively.

In summary, based on data samples collected between $\sqrt{s} = 4.21$ and 4.42 GeV collected with the BESIII detector, the process $e^+e^- \rightarrow \omega\chi_{c0}$ is observed at $\sqrt{s} = 4.23$ and 4.26 GeV for the first time, and the Born cross sections are measured to be $(55.4 \pm 6.0 \pm 5.9)$ and $(23.7 \pm 5.3 \pm 3.5)$ pb, respectively. For other energy points, no significant signals are found and upper limits on the cross section at the 90% C.L. are determined. The data reveals a sizeable $\omega\chi_{c0}$ production around 4.23 GeV/ c^2 as predicted in Ref. [11]. By assuming the $\omega\chi_{c0}$ signals come from a single resonance, we extract the $\Gamma_{ee}\mathcal{B}(\omega\chi_{c0})$, mass, and width of the resonance to be $(2.7 \pm 0.5 \pm 0.4)$ eV, $(4230 \pm 8 \pm 6)$ MeV/ c^2 , and $(38 \pm 12 \pm 2)$ MeV, respectively. The parameters are inconsistent with those obtained by fitting a single resonance to the $\pi^+\pi^- J/\psi$ cross section [1]. This suggests that the observed $\omega\chi_{c0}$ signals are unlikely from the $Y(4260)$. The $e^+e^- \rightarrow \omega\chi_{c1,2}$ channels are also searched for, but no significant signals are observed; upper limits at the 90% C.L. on the production cross sections are determined. By comparing with our $\omega\chi_{c0}$ results, the measured $e^+e^- \rightarrow \omega\chi_{c1,2}$ cross sections are found to be much lower than the predictions in Ref. [12].

The BESIII collaboration thanks the staff of BEPCII and the IHEP computing center for their strong support. This work is supported in part by National Key Basic Research Program of China under Contract No. 2015CB856700; Joint Funds of the National Natural Science Foundation of China under Contracts Nos. 11079008, 11179007, U1232201, U1332201; National Natural Science Foundation of China (NSFC) under Contracts Nos. 10935007, 11121092, 11125525, 11235011, 11322544, 11335008; the Chinese Academy of Sciences (CAS) Large-Scale Scientific Facility Program; CAS under Contracts Nos. KJCX2-YW-N29, KJCX2-YW-N45; 100 Talents Program of CAS; German Research Foundation DFG under Contract No. Collaborative Research Center CRC-1044; Istituto Nazionale di Fisica Nucleare, Italy; Ministry of Development of Turkey under Contract No. DPT2006K-120470; Russian Foundation for Basic Research under Contract No. 14-07-91152; U. S. Department of Energy under Contracts Nos. DE-FG02-04ER41291, DE-FG02-05ER41374, DE-FG02-94ER40823, DESC0010118; U.S. National Science Foundation; University of Groningen (RuG) and the Helmholtzzentrum fuer Schwerionenforschung GmbH (GSI), Darmstadt; WCU Program of National Research Foundation of Korea under Contract No. R32-2008-000-10155-0.

[1] B. Aubert *et al.* [BaBar Collaboration], Phys. Rev. Lett. **95**, 142001 (2005).

[2] G. Pakhlova *et al.* [Belle Collaboration], Phys. Rev. Lett.

TABLE III. The systematic uncertainties in the $\omega\chi_{c0}$ cross section measurement at each energy point (in %). The dashes mean not available.

Source/ \sqrt{s} (GeV)	4.21	4.22	4.23	4.245	4.26	4.31	4.36	4.39	4.42
Luminosity	1.0	1.0	1.0	1.0	1.0	1.0	1.0	1.0	1.0
Tracking	4.0	4.0	4.0	4.0	4.0	4.0	4.0	4.0	4.0
Photon	2.0	2.0	2.0	2.0	2.0	2.0	2.0	2.0	2.0
Kinematic fit	0.8	0.7	1.2	0.7	1.7	1.0	1.6	1.5	1.3
Angular distribution	0.5	0.5	1.0	0.8	0.5	1.5	1.9	2.3	2.5
Cross feed	1.1	1.0	0.7	1.1	1.0	1.3	1.2	1.3	1.4
Radiative factor	14.6	4.7	2.3	6.4	10.2	5.1	8.0	0.7	7.1
Fit Range	-	-	4.5	-	2.9	-	-	-	-
Background shape	-	-	2.4	-	7.2	-	-	-	-
Branching fraction	3.8	3.9	7.5	3.8	5.4	3.8	3.8	3.9	3.8
sum	16.1	7.8	10.6	8.9	14.8	8.1	10.4	6.7	9.8

- 98, 092001 (2007).
- [3] M. Ablikim *et al.* [BESIII Collaboration], Phys. Rev. Lett. **110**, 252001 (2013).
- [4] Z. Q. Liu *et al.* [Belle Collaboration], Phys. Rev. Lett. **110**, 252002 (2013).
- [5] T. Xiao, S. Dobbs, A. Tomaradze and K. K. Seth, Phys. Lett. B **727**, 366 (2013).
- [6] M. Ablikim *et al.* [BESIII Collaboration], Phys. Rev. Lett. **112**, 022001 (2014).
- [7] M. Ablikim *et al.* [BESIII Collaboration], Phys. Rev. Lett. **111**, 242001 (2013).
- [8] M. Ablikim *et al.* [BESIII Collaboration], arXiv:1409.6577.
- [9] M. Ablikim *et al.* [BESIII Collaboration], Phys. Rev. Lett. **112**, 132001 (2014).
- [10] N. Brambilla *et al.* [Quarkonium Working Group], Eur. Phys. J. C **71**, 1534 (2011).
- [11] L. Y. Dai, M. Shi, G. Y. Tang, H. Q. Zheng, arXiv:1206.6911v2.
- [12] L. Ma, X. H. Liu, X. Liu, S. L. Zhu, arXiv:1406.6879.
- [13] M. Ablikim *et al.* [BESIII Collaboration], Nucl. Instrum. Meth. A **614**, 345 (2010).
- [14] S. Agostinelli *et al.* [GEANT4 Collaboration], Nucl. Instrum. Meth. A **506**, 250 (2003).
- [15] D. J. Lange, Nucl. Instrum. Meth. A **462**, 152 (2001).
- [16] S. Jadach, B. F. L. Ward and Z. Was, Comp. Phys. Commun. **130**, 260 (2000); Phys. Rev. D **63**, 113009 (2001).
- [17] H. Albrecht *et al.* [ARGUS Collaboration], Phys. Lett. B **241**, 278 (1990).
- [18] J. Beringer *et al.* [Particle Data Group], Phys. Rev D **86**, 010001 (2012).
- [19] E. A. Kuraev and V. S. Fadin, Sov. J. Nucl. Phys. **41**, 466 (1985) [Yad. Fiz. **41**, 733 (1985)].
- [20] S. Actis *et al.* Eur. Phys. J. C **66**, 585 (2010).
- [21] W. A. Rolke, A. M. Lopez and J. Conrad, Nucl. Instr. Meth. A **551**, 493 (2005).
- [22] M. Ablikim *et al.* [BESIII Collaboration], Phys. Rev. D **81**, 052005 (2010)
- [23] M. Ablikim *et al.* [BESIII Collaboration], Phys. Rev. D **87**, 012002 (2013).
- [24] E. V. Abakumova, *et al.*, Nucl. Instrum. Meth. A **659**, 21 (2011).